

The LOG-EXP formula of the wall

A single formula for the law of the wall and its application to wall-modelled large-eddy simulation

Fengshun Zhang (张风顺),^{1,2} Zhideng Zhou (周志登),^{1,3} Xiaolei Yang (杨晓雷),^{1,3, a)} and Huan Zhang (张欢)²

¹⁾*The State Key Laboratory of Nonlinear Mechanics, Institute of Mechanics, Chinese Academy of Sciences, Beijing 100190, China*

²⁾*Department of Mechanics and Engineering Science, Lanzhou University, Lanzhou 730000, China*

³⁾*School of Engineering Sciences, University of Chinese Academy of Sciences, Beijing 100049, China*

(Dated: 7 January 2022)

In this work, we propose a single formula for the law of the wall, which is dubbed as the logarithmic-exponential (LOG-EXP) formula, for predicting the mean velocity profile in different regions near the wall. And then a feedforward neural network (FNN), whose inputs and training data are based on this new formula, is trained for the wall-modelled large-eddy simulation (WMLES) of turbulent channel flows. The direct numerical simulation (DNS) data of turbulent channel flows is used to evaluate the performance of both the formula and the FNN. Compared with the Werner-Wengle (WW) model for the WMLES, a better performance of the FNN for the WMLES is observed for predicting the Reynolds stresses.

^{a)}Electronic mail: xyang@imech.ac.cn

I. INTRODUCTION

The law of the wall is one of the cornerstones in wall-bounded turbulent flows^{1,2}. Different formulae have been proposed in the literature for the law of the wall. Roughly, they can be divided into two groups, i.e., the piecewise formulae and the single formulae. In the early year, the piecewise function was developed to describe the dynamics in different near-wall regions of the inner layer (e.g., for turbulent channel flows, it is located in the range of $0 \leq y \leq 0.1\delta$, where y denotes the wall-normal direction and δ is the half-height of the channel)^{3–10}, which includes the viscous sublayer, the buffer layer and the logarithmic layer¹. The most widely used law of the wall describes the viscous sublayer using the linear profile, i.e.,

$$U^+ = y^+, \quad (1)$$

where $U^+ = U/u_\tau$, $y^+ = y/\delta_v$ with the friction velocity $u_\tau = \sqrt{\tau_w/\rho}$ (where τ_w is the wall shear stress and ρ is the fluid density) and the viscous scale $\delta_v = \nu/u_\tau$ (ν is the kinematic viscosity of the fluid), and the logarithmic layer using the logarithmic law, i.e.,

$$U^+ = \frac{1}{\kappa} \ln(y^+) + 5.0, \quad (2)$$

where $\kappa = 0.4$ is the Kármán constant. A list of different piecewise formulae proposed in the literature for the law of the wall is shown in Table I. There are two disadvantages of the piecewise formulae: 1) the velocity in the buffer layer is not accurately described; 2) the velocity derivative is discontinuous because of the piecewise nature of these formulae. To resolve these two issues, different types of the law of the wall based on single formula have been proposed in the literature, which are often of two forms, i.e., the analytical form^{11–16} and the numerical form^{17,18}. The analytical forms are usually complicated or do not have a sound prediction^{12,14–16}, while the numerical forms have a better prediction of the velocity profile^{17,18}, but do not have a clear physical meaning or difficult to use in practice. Different single formulae for the law of the wall proposed in the literature are shown in Table II and Table III.

In this work, we propose a new single formula named as the logarithmic-exponential (LOG-EXP) formula shown as follows:

$$U^+(y^+) = \frac{1}{\kappa} \ln(1 + \kappa y^+) + A \left(1 - e^{-\frac{y^+}{B}}\right) + C \left(1 - e^{-\frac{y^+}{D}}\right), \quad (3)$$

where $A = 11.630$, $B = 7.194$, $C = -4.472$ and $D = 2.766$, validate the proposed formula using direct numerical simulation (DNS) data²⁸, the experimental data from other canonical wall

Authors	Formulae
Prandtl ³	$U^+ = y^+$ for $0 \leq y^+ \leq 11.5$
Taylor ⁴	$U^+ = 2.5 \ln(y^+) + 5.5$ for $11.5 \leq y^+$
Von Karman ⁵	$\begin{cases} U^+ = y^+, \text{ for } 0 \leq y^+ < 5 \\ U^+ = 5 \ln(y^+) - 3.05 \text{ for } 5 \leq y^+ < 30 \\ U^+ = 2.5 \ln(y^+) + 5.5 \text{ for } 30 \leq y^+ \end{cases}$
Deissler ⁶	$\begin{cases} U^+ = \int_0^{y^+} \left[1 + n^2 U^+ y^+ \left(1 - e^{-n^2 U^+ y^+} \right) \right]^{-1} dy^+, \text{ where } n = 0.124 \text{ for } 0 \leq y^+ < 26 \\ U^+ = 2.78 \ln(y^+) + 3.8, \text{ for } 26 \leq y^+ \end{cases}$
Rannie ⁷	$\begin{cases} U^+ = 1.454 \tanh(0.0688 y^+) \text{ for } 0 \leq y^+ < 27.5 \\ U^+ = 2.5 \ln(y^+) + 5.5 \text{ for } 27.5 \leq y^+ \end{cases}$
Breuer & Rodi ⁸	$\begin{cases} U^+ = y^+ \text{ for } 0 \leq y^+ < 5 \\ U^+ = A \ln(y^+) + B, \\ \quad \text{where } A = [k^{-1} \ln(30E) - 5] / \ln(6), B = 5 - A \ln(5) \text{ for } 5 \leq y^+ < 30 \\ U^+ = k^{-1} \ln(E y^+), \text{ where } E = 9.8 \text{ for } 30 \leq y^+ \end{cases}$
Werner & Wengle ⁹	$\begin{cases} U^+ = y^+ \text{ for } 0 \leq y^+ < 11.81 \\ U^+ = A (y^+)^B, \text{ where } A = 8.3, B = 1/7 \text{ for } 11.81 \leq y^+ \end{cases}$
Inagaki et al. ¹⁰	$\begin{cases} U^+ = y^+ \text{ for } 0 \leq y^+ < y_{C_1}^+ \\ U^+ = A_1 (y^+)^{B_1}, \text{ where } A_1 = 2.7, B_1 = 1/2, y_{C_1}^+ = A_1^{1/(1-B_1)} \text{ for } y_{C_1}^+ \leq y^+ < y_{C_2}^+ \\ U^+ = A_2 (y^+)^{B_2}, \text{ where } A_2 = 8.6, B_2 = 1/7, y_{C_2}^+ = (A_2/A_1)^{1/(B_1-B_2)} \text{ for } y_{C_2}^+ \leq y^+ \end{cases}$

TABLE I. Formulae for the law of the wall: piecewise function.

48 bounded flows^{29–31} and the classic law of the wall (i.e., Eq. (1) and Eq. (2)), and apply the new
49 single formula to wall-modelled large-eddy simulation (WMLES) via a feedforward neural net-
50 work (FNN) model for explicitly computing the wall shear stress using the wall-normal distance
51 and streamwise velocity.

52 The rest of this paper is organized as follows: in section II, the derivation process of the LOG-
53 EXP formula is presented; the proposed formula is validated using the DNS data of turbulent
54 channel flows and the experimental data of other canonical wall bounded flows in section III; then
55 it is applied WMLES via a feedforward neural network in section V; at last, conclusions are drawn

Authors	Formulae
Reichardt ¹¹	$U^+ = 2.5 \ln(1 + 0.4y^+) + 7.8 \left(1 - e^{-\frac{y^+}{11}} - \frac{y^+}{11} e^{-0.33y^+}\right)$
Spalding ¹²	$f(U^+) = U^+ + e^{-A} \left(e^{\kappa U^+} - 1 - \kappa U^+ - \frac{(\kappa U^+)^2}{2!} - \frac{(\kappa U^+)^3}{3!} - \frac{(\kappa U^+)^4}{4!}\right)$
Rasmussen ¹³	$y^+ = f(U^+)$, where $f(U^+) = U^+ + e^{-A} \left(2 \cosh(\kappa U^+) - (\kappa U^+)^2 - 2\right)$, $A = 2.2$, $\kappa = 0.4$
Musker ¹⁴	$U^+ = 5.424 \tan^{-1} \left[\frac{2y^+ - 8.15}{16.7} \right] + \log_{10} \left[\frac{(y^+ + 10.6)^{9.6}}{(y^+ - 8.15y^+ + 86)^2} \right] - 3.52 +$ $2.44 \left\{ \Pi \left[6 \left(\frac{y}{\delta} \right)^2 - 4 \left(\frac{y}{\delta} \right)^3 \right] + \left[\left(\frac{y}{\delta} \right)^2 \left(1 - \frac{y}{\delta} \right) \right] \right\}$, $\Pi = 0.55$
Dean ¹⁵	$y^+ e^{\kappa g(\Pi, \frac{y}{\delta})} = f(U^+)$, $g(\Pi, \frac{y}{\delta}) = \frac{1}{\kappa} (1 + 6\Pi) \left(\frac{y}{\delta} \right)^2 - \frac{1}{\kappa} (1 + 4\Pi) \left(\frac{y}{\delta} \right)^3$ where $f(U^+)$ is given by Spalding or Rasmussen's expressions listed above
Monkewitz, Chauhan and Nagib ¹⁶	$U_{\text{inner}}^+ = U_{\text{inner}, 23}^+ + U_{\text{inner}, 25}^+$ $U_{\text{inner}, 23}^+ = 0.68285472 \ln(y^{+2} + 4.7673096y^+ + 9545.9963) +$ $1.2408249 \arctan(0.010238083y^+ + 0.024404056) +$ $1.2384572 \ln(y^+ + 95.232690) - 11.930683$ $U_{\text{inner}, 25}^+ = -0.50435126 \ln(y^{+2} - 7.8796955y^+ + 78.389178) +$ $4.7413546 \arctan(0.12612158y^+ - 0.49689982)$ $-2.7768771 \ln(y^{+2} + 16.209175y^+ + 933.16587) +$ $0.37625729 \arctan(0.033952353y^+ + 0.27516982) +$ $6.5624567 \ln(y^+ + 13.670520) + 6.1128254$
van Driest ¹⁷	$U^+ = \int_0^{y^+} 2 \left[1 + \sqrt{1 + 0.64y^{+2} \left(1 - e^{-\frac{y^+}{26}}\right)^2} \right]^{-1} dy^+$
Duprat et al. ¹⁸	$\frac{\partial U^+}{\partial y^+} = \frac{\text{sign}(\frac{\partial P}{\partial x})(1 - \alpha)^{3/2} y^+ + \text{sign}(\tau_w) \alpha}{1 + \frac{y^+}{v}}$ $\frac{v}{v} = ky^+ \left[\alpha + y^+ (1 - \alpha)^{3/2} \right]^\beta \left(1 - e^{-y^+/(1 + A\alpha^3)} \right)^2$, where $\beta = 0.78$, $A = 17$, $\alpha = 1$
Cantwell ¹⁹	$U^+(y^+) = \int_0^{y^+} \left(-\frac{1}{2\lambda(s)^2} + \frac{1}{2\lambda(s)^2} \left(1 + 4\lambda(s)^2 \left(1 - \frac{s}{R_\tau} \right) \right)^{1/2} \right) ds$ $\lambda(y^+) = \frac{\kappa y^+ (1 - e^{-(y^+/a)^m})}{\left(1 + \left(\frac{y^+}{bR_\tau} \right)^n \right)^{1/n}}$, where $k = 0.4092$, $a = 20.095$, $m = 1.621$, $b = 0.3195$, $n = 1.619$.
Rotta ²⁰	$U^+ = \frac{1}{2\kappa I_m^+} \left(1 - \sqrt{1 + 4I_m^{+2}} \right) + \frac{1}{\kappa} \ln \left(2I_m^+ + \sqrt{1 + 4I_m^{+2}} \right) + \delta_l^+$, where $I_m = \kappa(y - \delta_l)$, $I_m^+ = u_\tau I_m / v$ and $\delta_l^+ = u_\tau \delta_l / v$ $\delta_l^+ = 5.0$ and experimental data ^{21,22} suggests $\delta_l^+ = 7.0$.

TABLE II. Formulae for the law of the wall: single formula.

Authors	Formulae
Nickels ²³	$U^+ = y_c^+ \left[1 - \left(1 + 2(y^+/y_c^+) + \frac{1}{2}(3 - p_x^+ y_c^+)(y^+/y_c^+)^2 - \frac{3}{2}p_x^+ y_c^+ (y^+/y_c^+)^3 \right) e^{-3y^+/y_c^+} \right] +$ $\frac{\sqrt{1+p_x^+ y_c^+}}{6\kappa_o} \ln \left(\frac{1+(0.6(y^+/y_c^+))^6}{1+\eta^6} \right) + b \left(1 - e^{-\frac{5(\eta^4+\eta^8)}{1+5\eta^3}} \right), \text{ where } \eta = y/\delta, p_x^+ = (\nu/\rho U_\tau^3)/(dp/dx),$ $p_x^+ y_c^{+3} + y_c^{+2} - R_c^2 = 0, R_c = \frac{U_T y_c}{\nu} \text{ and } U_T = \sqrt{\tau(y = y_c)/\rho}$
Haritonidis ²⁴	$U^+ = \frac{1}{\lambda} \arctan \lambda y^+ - \frac{a}{2\lambda^2} \ln \left(1 + \lambda^2 y^{+2} \right), \text{ where } \lambda^2 = \alpha f^+, \alpha = \frac{nm^2}{2}, a = 1/h^+,$ <p>n is the number of ejections of equal strength, $f = 1/\Delta t_b$ is the bursting frequency,</p> $m = \kappa n^{-1} (\Delta t_e / \delta t_b)^{-1} \text{ and } \Delta t_e \text{ is the duration of the ejections.}$
Yakhot et al. ²⁵	$U^+(y^+) = \frac{1}{3\kappa} \left[4C^{1/4} - z + \ln \left(\frac{z+1}{z-1} \right) + 2 \arctan(z) - \ln \left(\frac{C^{1/4}+1}{C^{1/4}-1} \right) - 2 \arctan(C^{1/4}) \right],$ <p>where $z = (\hat{v}^3 - 1 + C)^{1/4} / \hat{v}^{3/4}$ and $\hat{v}^4 + (C-1)\hat{v} - \hat{v}_m^4 = 0$,</p> $\hat{v} = v_t/\nu, \hat{v}_m = \kappa l^+, l^+ = u_\tau l/\nu.$
Nikuradse ²⁶	$U^+ = \int_0^{y^+} 2 \left(1 - \frac{y^+}{Re_\tau} \right) \left[1 + \sqrt{1 + 4l_m^{+2} \left(1 - \frac{y^+}{Re_\tau} \right)} \right]^{-1} dy^+,$ $\frac{l_m}{\delta} = 0.14 - 0.08 \left(1 - \frac{y^+}{Re_\tau} \right)^2 - 0.06 \left(1 - \frac{y^+}{Re_\tau} \right)^4$
Cebeci, Bradshaw ²⁷	$U^+ = \int_0^{y^+} 2 \left(1 - \frac{y^+}{Re_\tau} \right) \left[1 + \sqrt{1 + 4l_m^{+2} \left(1 - \frac{y^+}{Re_\tau} \right)} \right]^{-1} dy^+,$ $\frac{l_m}{\delta} = \left(0.14 - 0.08 \left(1 - \frac{y^+}{Re_\tau} \right)^2 - 0.06 \left(1 - \frac{y^+}{Re_\tau} \right)^4 \right) \left(1 - e^{-\frac{y^+}{26}} \right)$

TABLE III. Formulae for the law of the wall: single formula.

in section V.

II. DERIVATION OF THE LOG-EXP FORMULA OF THE WALL

To derive the single formula for the law of the wall, we propose the following expression for the first derivative of the mean streamwise velocity,

$$\frac{dU^+}{dy^+} = \frac{1}{1 + \kappa y^+} + \Phi(y^+) \quad (4)$$

where $\Phi(y^+)$ is the function to be given and satisfies these conditions, i.e., $\lim_{y^+ \rightarrow \infty} \Phi(y^+) = \lim_{y^+ \rightarrow 0} \Phi(y^+) = 0$. It is noticed that this expression exactly satisfies the boundary condition at the wall, i.e.,

$$\frac{dU^+}{dy^+} = 1 \text{ at } y^+ = 0, \quad (5)$$

and approximately satisfies the condition in the logarithmic layer, i.e.,

$$\frac{dU^+}{dy^+} = \frac{1}{\kappa y^+} \text{ for } y^+ \text{ in the logarithmic region,} \quad (6)$$

where y^+ is large enough such that the first term on the right-hand side of Eq. (4) can be approximated by $1/(\kappa y^+)$, and the second term on the right-hand side of Eq. (4) is considered being negligible.

There are many choices for $\Phi(y^+)$. In this work, we propose to use the following expression:

$$\Phi(y^+) = \frac{A}{B}e^{\frac{-y^+}{B}} + \frac{C}{D}e^{\frac{-y^+}{D}}, \quad (7)$$

where A, B, C , and D are constants satisfying the following constraint

$$\frac{A}{B} + \frac{C}{D} = 0. \quad (8)$$

We will try to explain the physical meaning of the two exponential terms in Eq. (7) after we set the values of A, B, C and D . To obtain the law of the wall, we first substitute Eq. (7) into Eq. (4), which yields

$$\frac{dU^+}{dy^+} = \frac{1}{1 + \kappa y^+} + \frac{A}{B}e^{\frac{-y^+}{B}} + \frac{C}{D}e^{\frac{-y^+}{D}}. \quad (9)$$

Then, the expression for U^+ is obtained by integrating Eq. (9) with respect to y^+ as follows:

$$U^+(y^+) = \frac{1}{\kappa} \ln(1 + \kappa y^+) + A \left(1 - e^{-\frac{y^+}{B}}\right) + C \left(1 - e^{-\frac{y^+}{D}}\right). \quad (10)$$

Finally, the values of A, B, C and D are determined by fitting Eq. (10) using the DNS data²⁸ of the turbulent channel flow at $Re_\tau = 5200$ with the constraint shown in Eq. (8). Specifically, the mean velocity values in the range of $0 \leq y \leq 0.1\delta$ are employed to obtain the parameters as follows: $A = 11.630, B = 7.194, C = -4.472$ and $D = 2.766$.

We examine different terms in Eq. (9) in figure 1. As seen, the velocity derivative captured by the first term on the right-hand side of Eq. (9), i.e., $1/(1 + \kappa y^+)$, is less than the actual gradient. The second term on the right-hand side of Eq. (9), i.e., the exponential term with a positive coefficient $(A/B)e^{-y^+/B}$, which increases as approaching the wall, takes into account the effect of increased turbulence as approaching the buffer layer region. The third term on the right-hand side of Eq. (9), i.e., the exponential term with a negative coefficient $(C/D)e^{-y^+/D}$, on the other hand, decreases as approaching the wall, which offsets the increase of the second term, and acts as a damping function in the near-wall region. It is noticed that we attempt to understand the effects of different terms in Eq. (9) instead of the exact physical interpretation of different terms.

The asymptotic behavior of the derived single formula is examined as follows. In the viscous sublayer, we expand Eq. (10) in Taylor series about $y^+ = 0$ and neglect the high order terms for

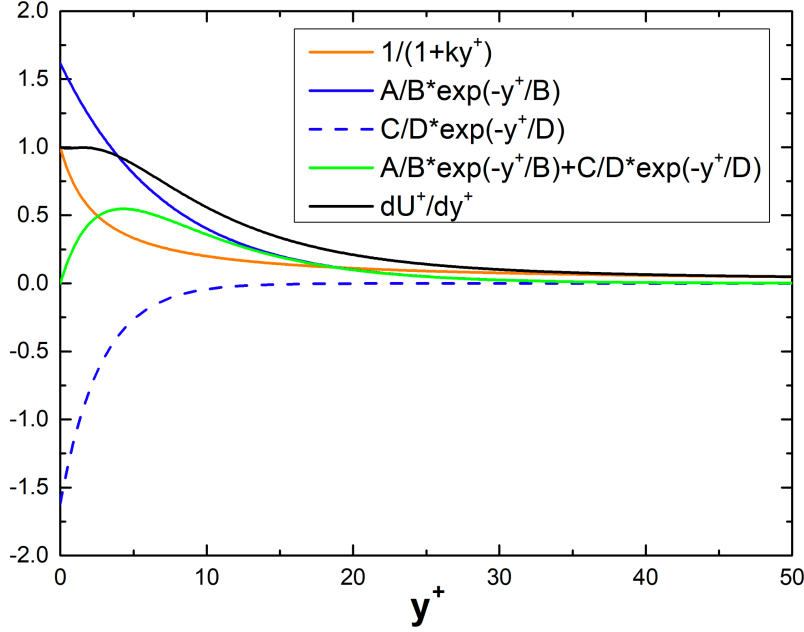


FIG. 1. Vertical variations of different terms in Eq. (10).

small y^+ and obtain the linear profile as follows:

$$\lim_{y^+ \rightarrow 0} U^+(y^+) \approx \lim_{y^+ \rightarrow 0} \left(y^+ + \frac{A}{B}y^+ + \frac{C}{D}y^+ \right) = y^+. \quad (11)$$

In the logarithmic region, where y^+ is large enough at high Reynolds numbers, the logarithmic law can be recovered from Eq. (10) shown as follows:

$$\lim_{y^+ \rightarrow \infty} U^+(y^+) \approx \frac{1}{\kappa} \cdot \ln(y^+) + A - \frac{D \cdot A}{B} + \frac{\ln(\kappa)}{\kappa} = \frac{1}{\kappa} \ln(y^+) + 4.9 \quad (12)$$

considering that $\lim_{y^+ \rightarrow \infty} \ln(\kappa + y^+) \approx \ln(y^+)$ and $\lim_{y^+ \rightarrow \infty} e^{-\frac{y^+}{B}} \approx \lim_{y^+ \rightarrow \infty} e^{-\frac{y^+}{D}} \approx 0$.

III. VALIDATION OF THE LOG-EXP FORMULA

In this section we validate the proposed LOG-EXP formula, i.e., Eq. (10), using the DNS data of turbulent channel flow²⁸, the experimental data from other canonical wall bounded flows^{29–31}.

Figure 2(a) compares the predictions from several single formulae with the DNS data at $Re_\tau = 5200$, which are employed for calibrating the proposed formula. It is shown that all the formulae have a good prediction in the viscous sublayer and buffer layer. In the logarithmic region, which is enlarged and shown in Figure 2(b), the predictions of the proposed LOG-EXP formula collapse well with the DNS data, while some formulae, such as those predicted by Dean¹⁵, Reichardt¹¹,

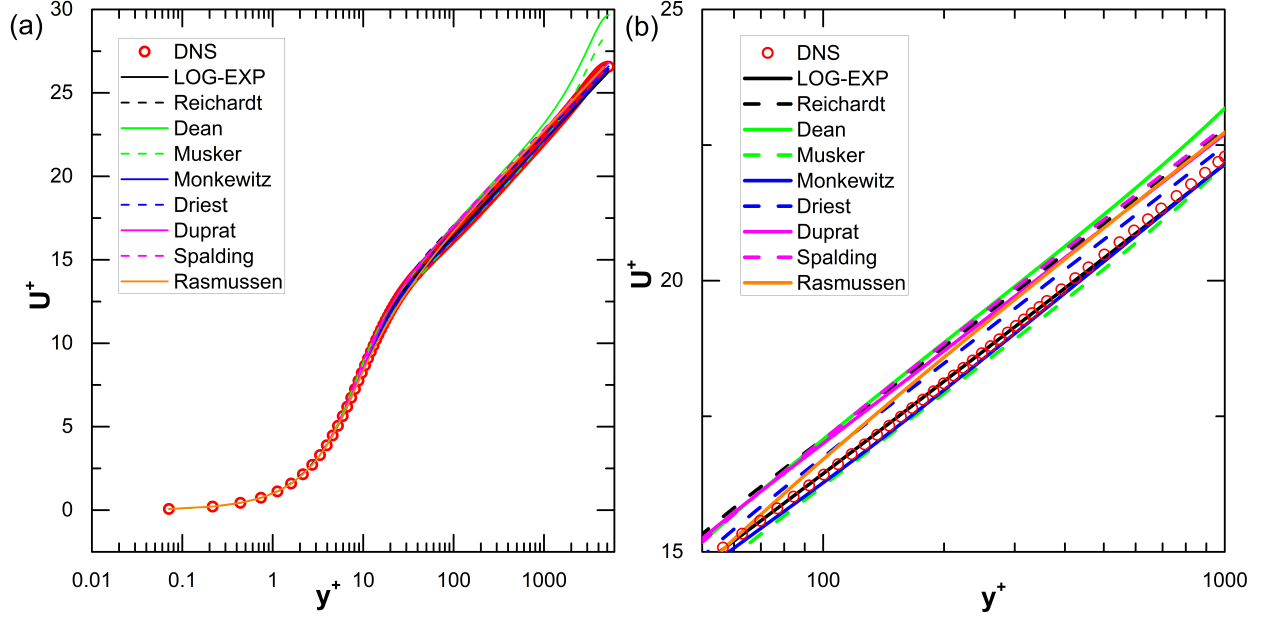


FIG. 2. (a) Comparison of the velocity profiles predicted by the LOG-EXP formula and others with that from DNS for the turbulent channel flow at Reynolds numbers $Re_\tau = 5200$ (b) Zoomed-in plot of (a) for $50 \leq y^+ \leq 1000$.

Spalding¹² and van Driest¹⁷, overpredict the velocity in this region. Furthermore, it is observed the predictions by Dean¹⁵ and Musker¹⁴ tend to deviate away from the DNS data. In Figure 3, we show the comparison of the first derivative of the velocity. As seen, predictions from different formulae agree well with the DNS data in the logarithmic layer and the outer layer. Discrepancies are observed in the viscous sublayer and buffer layer (i.e., $y^+ < 10$) for Reichardt's formula¹¹ and Dean's formula¹⁵, which overpredict the velocity derivative dU^+/dy^+ . The velocity derivative predicted by the proposed LOG-EXP formula, on the other hand, agrees well with DNS data for all vertical locations.

In Figure 4 and Figure 5, we compare predictions from the proposed LOG-EXP formula with the DNS data²⁸ for different Reynolds numbers. Although minor differences are observed for the low Reynolds number case with $Re_\tau = 180$, an overall good agreement is observed for both the velocity profile and the first derivative of dU^+/dy^+ for the proposed LOG-EXP formula.

To qualitatively evaluate the proposed LOG-EXP formula, we calculate the maximum absolute error of the velocity, which is defined by

$$e_{\max, U^+} = \max_{0 \leq y^+ \leq 0.3} \frac{|U_F^+ - U_{DNS}^+|}{\langle |U_{DNS}^+| \rangle}, \quad (13)$$

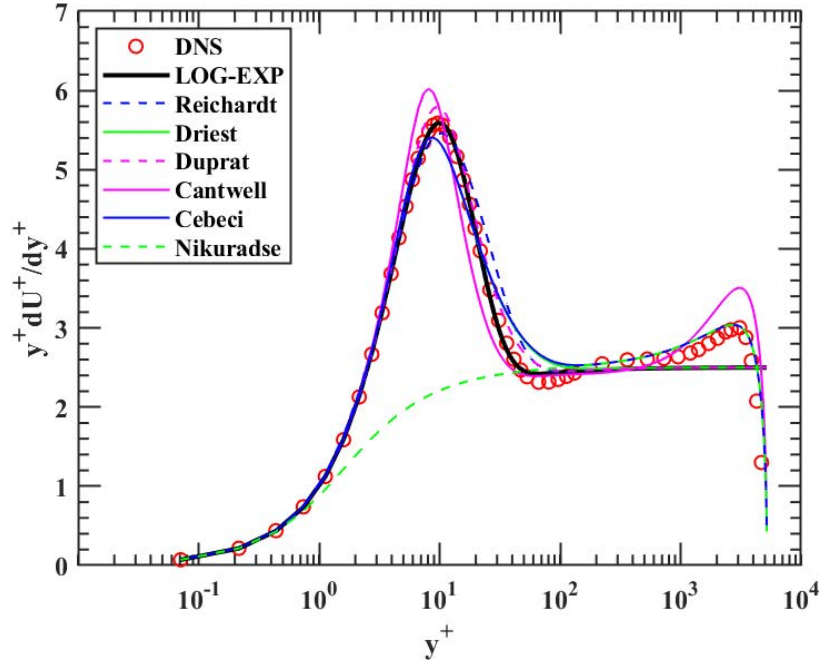


FIG. 3. Comparison of $y^+ dU^+/dy^+$ predicted by the LOG-EXP formula and others with that from DNS for the turbulent channel flow at Reynolds numbers $Re_\tau = 5200$.

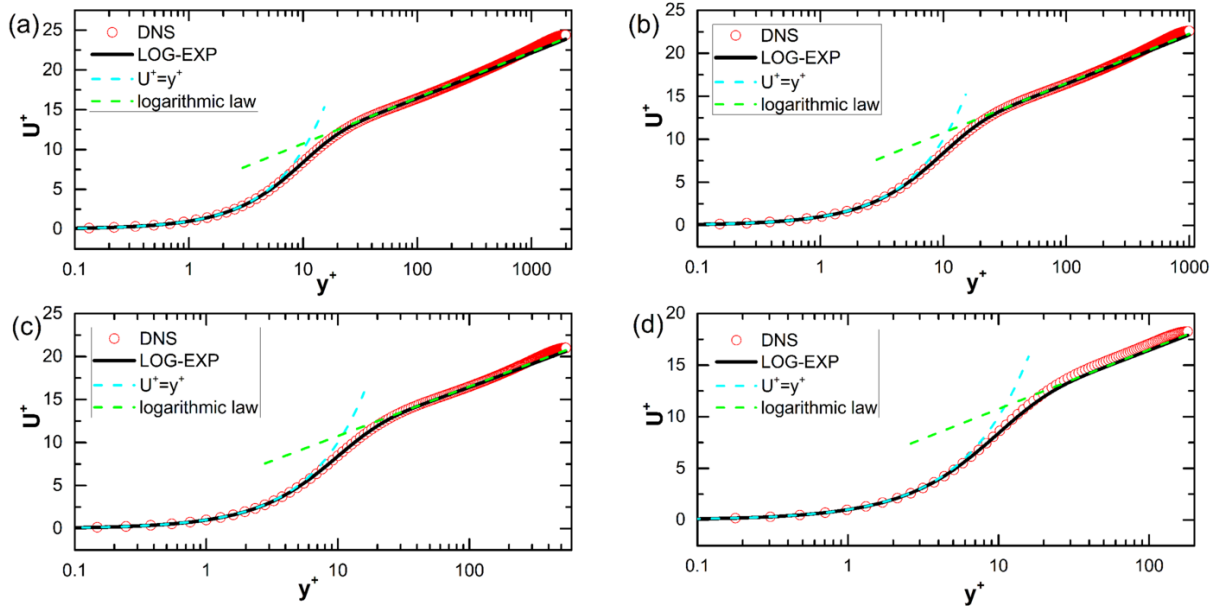


FIG. 4. Comparison of the velocity profiles predicted by the LOG-EXP formula with those from DNS for the turbulent channel flow with different Reynolds numbers for (a) $Re_\tau = 2000$, (b) $Re_\tau = 1000$, (c) $Re_\tau = 550$, and (d) $Re_\tau = 180$.

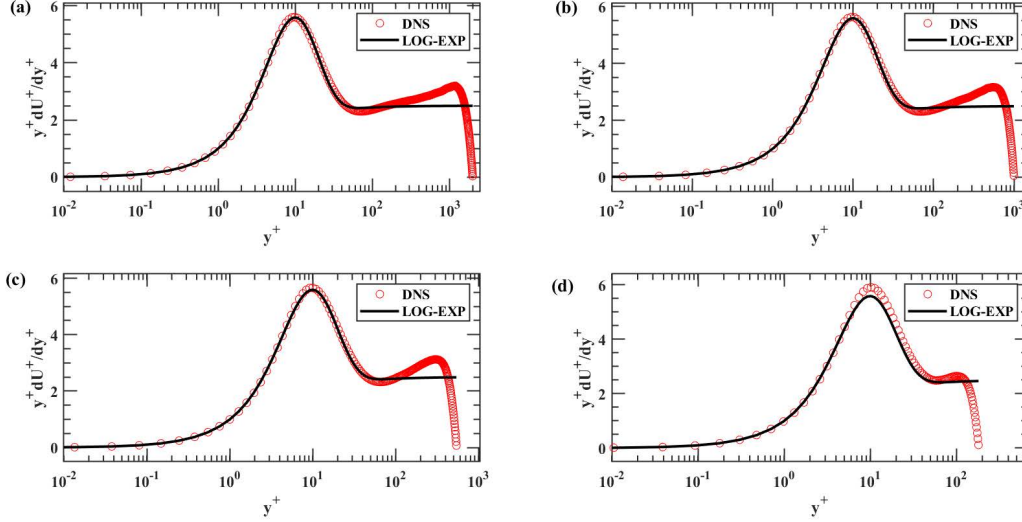


FIG. 5. Comparison of $y^+ dU^+/dy^+$ predicted by the LOG-EXP formula with those from DNS for the turbulent channel flow with different Reynolds numbers for (a) $Re_\tau = 2000$, (b) $Re_\tau = 1000$, (c) $Re_\tau = 550$, and (d) $Re_\tau = 180$.

where U_{DNS}^+ , U_F^+ and $\langle U_{DNS}^+ \rangle$ are the velocity of the DNS data, the velocity calculated by the single formula and the mean of U_{DNS}^+ averaged over $0.0 \leq y/\delta \leq 0.3$, and the maximum absolute error of dU^+/dy^+ , which is defined by

$$e_{\max, dU^+/dy^+} = \max_{0 \leq y/\delta \leq 0.3} \frac{\left| \left(\frac{dU^+}{dy^+} \right)_F - \left(\frac{dU^+}{dy^+} \right)_{DNS} \right|}{\left\langle \left| \left(\frac{dU^+}{dy^+} \right)_{DNS} \right| \right\rangle}, \quad (14)$$

where $(dU^+/dy^+)_{DNS}$, $(dU^+/dy^+)_F$ and $\langle (dU^+/dy^+)_{DNS} \rangle$ are the first derivative of the velocity of the DNS data, the first derivative of the velocity calculated from single formula and the mean value of $(dU^+/dy^+)_{DNS}$ averaged over $0.0 \leq y/\delta \leq 0.3$, respectively.

In Figure 6, we plot the errors of the velocity predicted by different formulae for different Reynolds numbers. As seen in Figure 6(a), the errors of the LOG-EXP predictions, which are less than 0.1, are lower than the other formulae except for the very low Reynolds number case. Figure 6(b) and (c) show the vertical location $y_{e_{\max, U^+}}$ where the e_{\max, U^+} occurs for different normalization, i.e., the viscous length scale δ_v and the channel half-height δ , respectively. It is observed that $y_{e_{\max, U^+}}$ increases with the increase of the Reynolds number when normalized using δ_v , while remains nearly constant for $y_{e_{\max, U^+}}$ when normalized using δ for the proposed LOG-EXP formula,

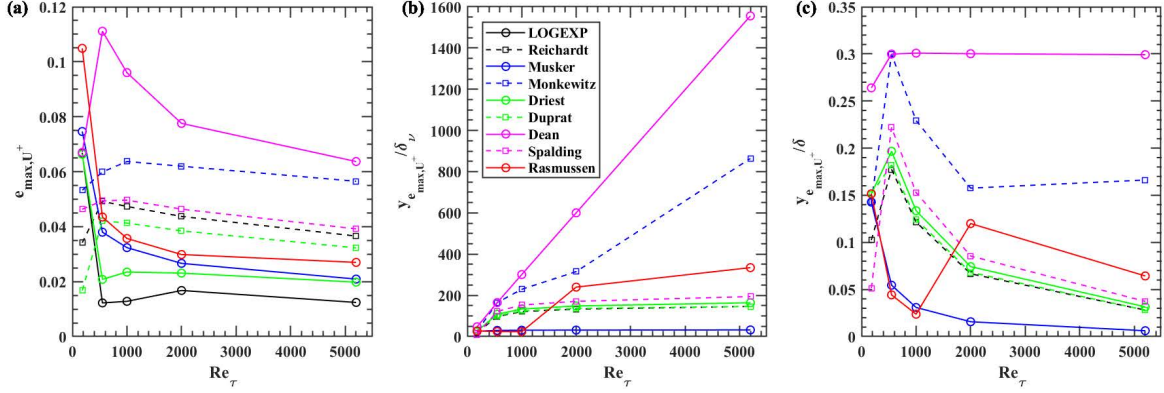


FIG. 6. (a) The maximum absolute error e_{\max, U^+} of the velocity predicted by different formulae compared with DNS data for different Reynolds numbers; (b) The vertical location in wall units $y_{e_{\max, U^+}}/\delta_\nu$ where the maximum absolute error occurs; (c) The vertical location normalized by the half-height of channel $y_{e_{\max, U^+}}/\delta$ where the maximum absolute error occurs.

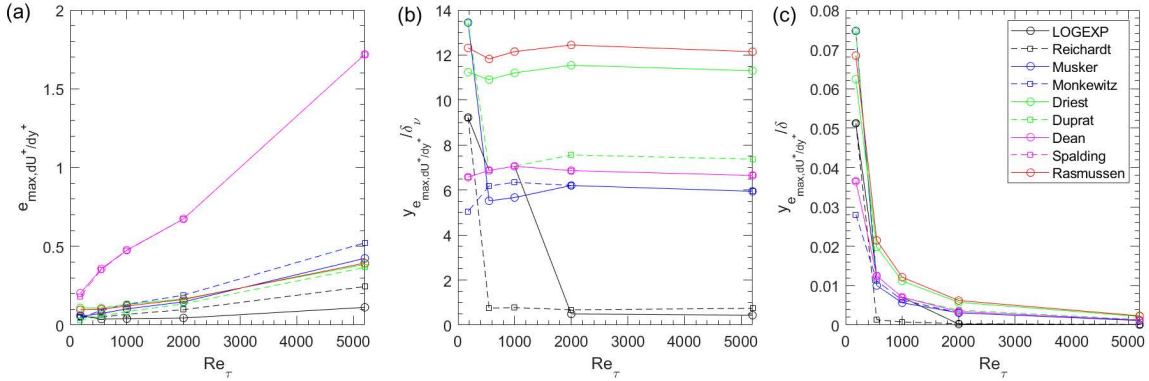


FIG. 7. Same as Figure 6 but for $e_{\max, dU^+/dy^+}$ and $y_{e_{\max, dU^+/dy^+}}$.

In Figure 7, the errors of the velocity derivatives predicted by different formulae are examined for different Reynolds numbers. As seen in Figure 7(a), the errors of the LOG-EXP predictions are lower than others, which increase via Reynolds number. Figure 7 (b) and (c) show the locations where the $e_{\max, dU^+/dy^+}$ occurs, which are normalized by the length scales δ_ν and δ , respectively. As seen, the $y_{e_{\max, dU^+/dy^+}}$ for velocity derivative is close to or within the viscous sublayer for different Reynolds numbers.

We further apply the proposed LOG-EXP formula to different types of canonical flows. Figure 8 shows the semi-logarithmic plots of mean velocity profiles in the circular pipe flow^{29,31} and the turbulent boundary layer on a flat plate³⁰. An overall good agreement between the LOG-EXP

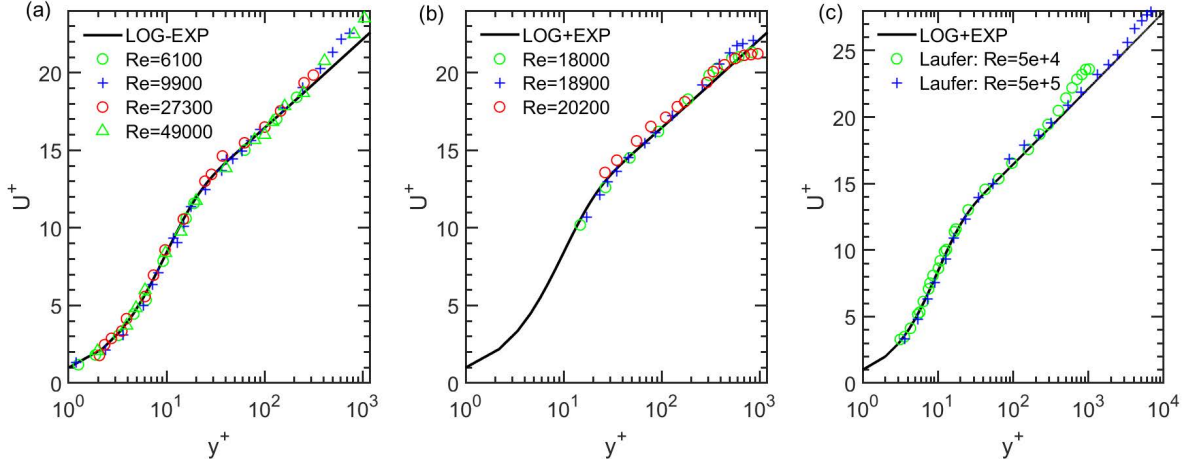


FIG. 8. Comparison of the velocity profiles predicted by the LOG-EXP formula with the experimental data from (a) Lindgren and Chao³¹, (b) Charnay et al.³⁰, (c) Laufer²⁹ for (a,c) the circular pipe flow and (b) the turbulent boundary layer on a flat plate.

formula and the experimental data is observed in the near wall region.

IV. APPLICATION OF THE LOG-EXP FORMULA TO WMLES

In this section, we apply the LOG-EXP formula to WMLES. In WMLES, the wall shear stress at the wall is often employed as approximate boundary conditions for outer flow simulations. However, the wall shear stress cannot be determined explicitly using the LOG-EXP formula. To address this issue, we employ the feedforward neural network (FNN) to construct an explicit LOG-EXP model for explicitly computing the wall shear stress (details on the model training and a priori test can be found in the appendix V. The explicit LOG-EXP model is then applied in WMLES and tested using turbulent channel flows at different Reynolds numbers.

The explicit LOG-EXP model is implemented in the large-eddy simulation module of the Virtual Flow Simulator (VFS-Wind) code^{32,33}. The governing equations are the incompressible Navier-Stokes equations, which are discretized spatially using the second-order central differencing scheme, and advanced in time using a second-order fractional step method. The subgrid-scale stress is modeled using the dynamic procedure³⁴. In the implementation of the LOG-EXP wall model, the wall-tangential component of the velocity and wall-normal distance as the second off-wall grid nodes are employed as inputs for the LOG-EXP model, with computed wall shear stresses employed as boundary conditions for the outer flow simulation. For the wall-normal component

of the velocity, a no-slip boundary condition is employed.

Two cases with different Reynolds numbers are considered, i.e., the Reynolds number defined using the friction velocity $Re_\tau = 1000, 5200$. For both cases, the computational domain is $L_x \times L_y \times L_z = 7.0m \times 2.0m \times 3.5m$ in the streamwise, vertical and spanwise directions, respectively, with the corresponding numbers of grid nodes $N_x \times N_y \times N_z = 33 \times 33 \times 33$, which are uniformly distributed in all three directions.

We compare the predictions from WMLES with the LOG-EXP model with the DNS results³⁵ and those from the Werner-Wengle (WW) model⁹. It is shown in Figure 9 (a) that the mean velocity profiles predicted by the WW model and the LOG-EXP model agree well with the DNS profile. For the primary Reynolds shear stress $\langle u'v' \rangle^+$, figure 9 (b) shows that the WW model somewhat overestimates the magnitude of $\langle u'v' \rangle^+$ for $200 < y^+ < 800$, which, on the other hand, is accurately predicted by the LOG-EXP model. The comparisons of the normal Reynolds stresses are shown in Figure 9 (c, d). It is observed that both wall models overpredict the streamwise component of the normal Reynolds stress $\langle u'u' \rangle^+$, while underpredict the wall-normal component $\langle v'v' \rangle^+$. Comparisons for the case with $Re_\tau = 5200$ are shown in Figure 10, with similar observations as for the case with $Re_\tau = 1000$.

V. CONCLUSIONS

In this work, we proposed a new single formula for the law of the wall, which is dubbed as the LOG-EXP formula. It is derived based on the decomposition of the velocity derivative into a term satisfying the boundary conditions of the velocity derivative at the wall and in the logarithmic region, and two exponential terms accounting for the increase of turbulence as approaching the buffer layer and the viscous damping effect in the near-wall region, respectively. The derived LOG-EXP formula, which is composed of a logarithmic term and two exponential terms, works for the whole inner layer region and gives continuous predictions of both velocity and velocity derivative. Its capability is evaluated using DNS data of turbulent channel flows and some other canonical wall-bounded turbulent flows at different Reynolds numbers. Good agreements are obtained for all the considered cases.

The proposed LOG-EXP formula is then applied to WMLES. To avoid the cost of solving the LOG-EXP expression for the friction velocity, an explicit LOG-EXP model is developed using the feedforward neural network for computing wall shear stress for WMLES. The WMLES with the

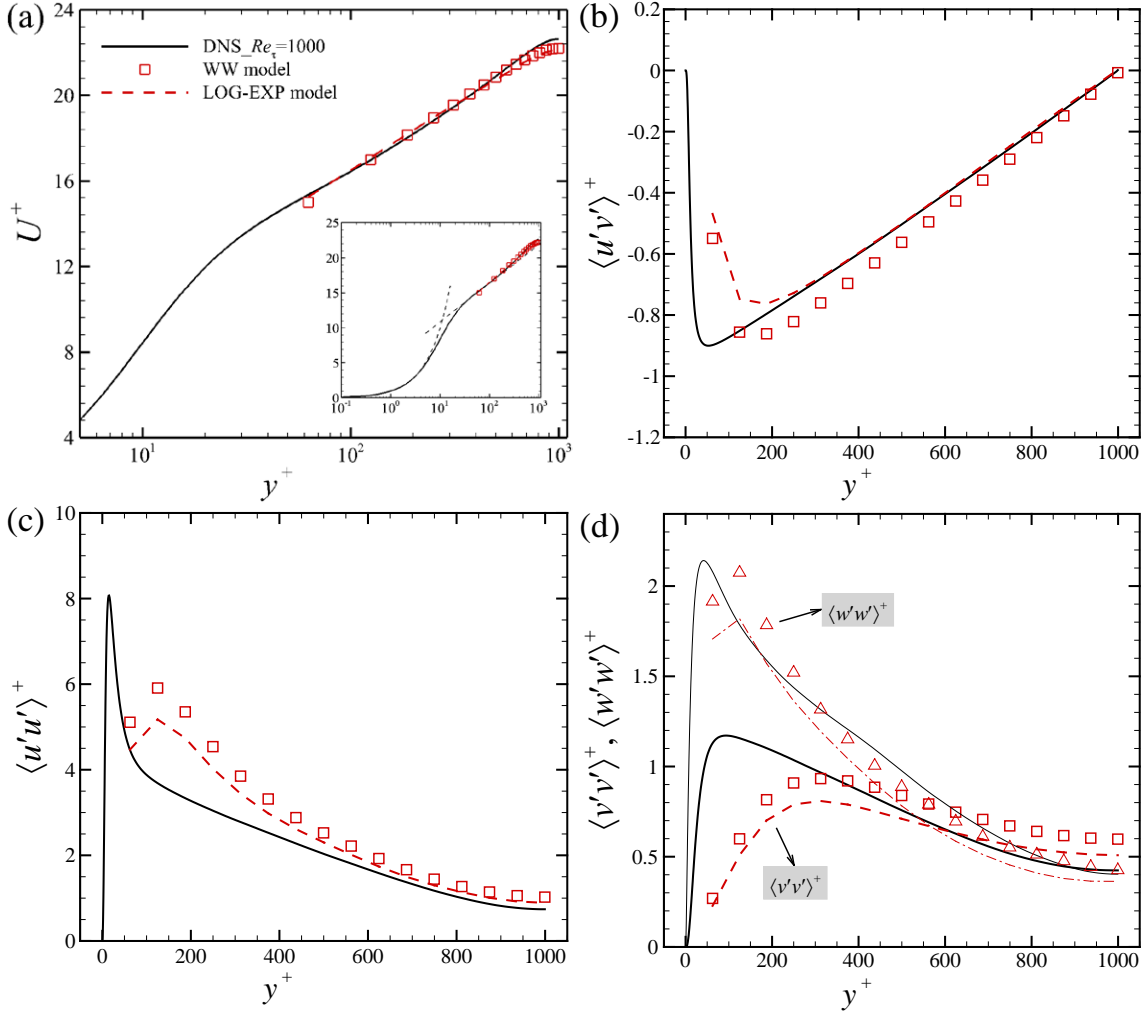


FIG. 9. Comparison of predictions from the WMLES with the LOG-EXP model with DNS and those from the WW model for (a) the mean streamwise velocity, (b) the primary Reynolds shear stress $\langle u'v' \rangle^+$, and (c, d) the normal Reynolds stresses $\langle u'u' \rangle^+$, $\langle v'v' \rangle^+$ and $\langle w'w' \rangle^+$, respectively.

LOG-EXP model is evaluated using the DNS data of turbulent channel flows. An overall good agreement is obtained for both mean streamwise velocity and the Reynolds stresses.

ACKNOWLEDGEMENTS

This work is partially supported by NSFC Basic Science Center Program for “Multiscale Problems in Nonlinear Mechanics” (NO. 11988102).

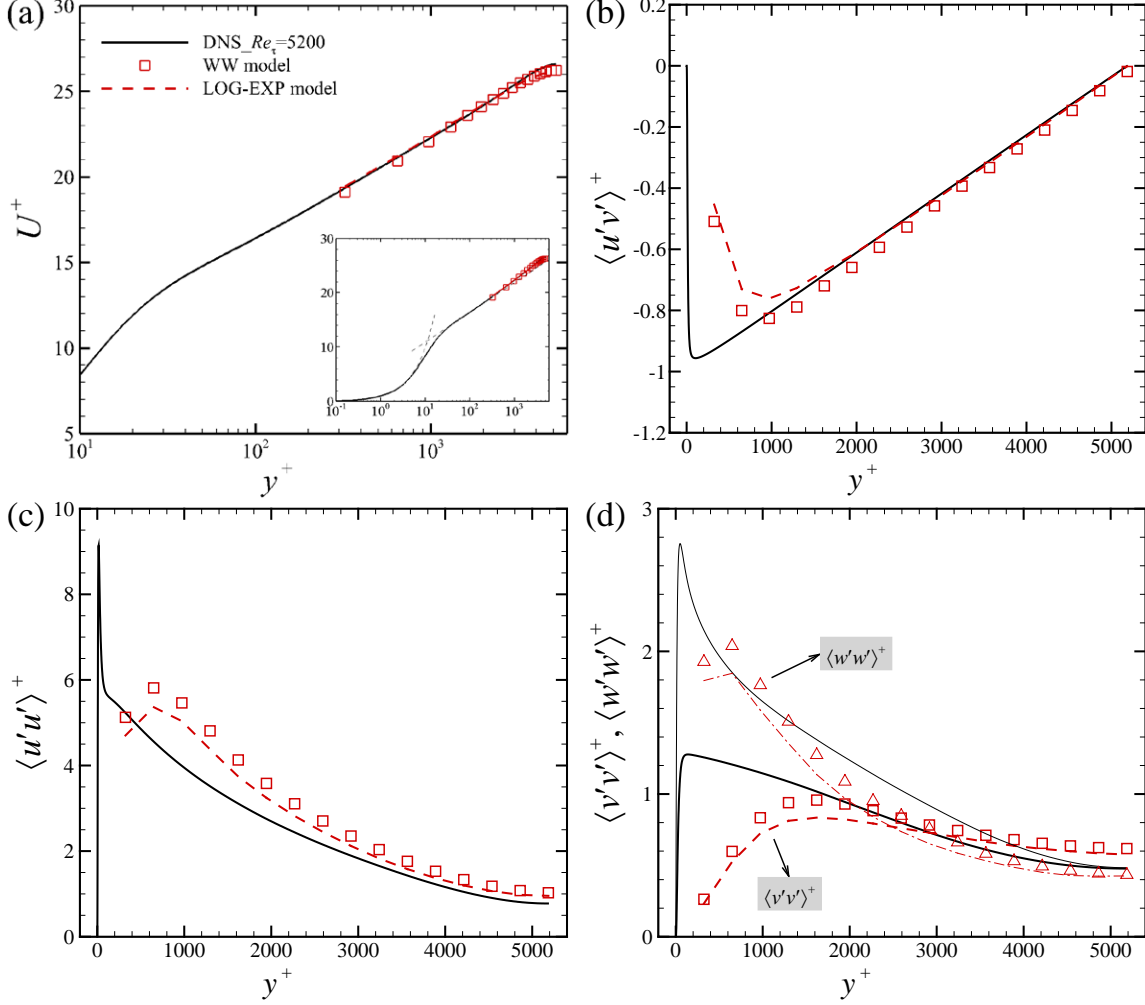


FIG. 10. The same as figure 9 but for $Re_\tau = 5200$.

DATA AVAILABILITY

The data that support the findings of this study are available from the corresponding author upon reasonable request.

APPENDIX A: A NEURAL NETWORK MODEL FOR EXPLICITLY COMPUTING WALL SHEAR STRESS

In this appendix, we describe the procedure for constructing a neural network model for explicitly computing the wall shear stress using the wall-normal distance and the streamwise velocity, which can be used directly in WMLES without the need to solve the implicit LOG-EXP formula.

As shown in Figure 11, a multi-hidden-layer feedforward neural network is employed for the construction of the explicit model, which contains an input layer, multi hidden layers and an output layer. Each layer has a number of neurons, which are computational units that take weighted sums of the inputs to an activation function and calculate the output. Then the outputs of each layer are fed forward as inputs to the next layer. The training goal of the neural network is to find the optimal weight and bias coefficients to minimize the loss of the neural network. More details about the neural network can be found in the reference³⁶.

The structure of the neural network employed in this work is shown in Tabel IV. The activation function used in this paper is the hyperbolic tangent function (tanh), which is defined as follows:

$$f(x) = \frac{e^x - e^{-x}}{e^x + e^{-x}}. \quad (15)$$

The input and output data are normalized using the Min-Max scaling,

$$x^* = \frac{x - x_{min}}{x_{max} - x_{min}}. \quad (16)$$

The loss function of the neural network is set as the mean square error (MSE), which is defined as follows:

$$L_{FNN} = \frac{1}{N_s} \sum_{i=1}^{N_s} (y_i - y_i^*)^2, \quad (17)$$

where N_s is the number of training samples, y_i and y_i^* are the FNN output and the labeled output from the training data, respectively. Besides, the error back-propagating (BP) scheme³⁷ and the Adam optimizer³⁸ are implemented with Keras³⁹ to train the FNN model.

The training data is obtained by solving the Eq. (3) about the friction velocity u_τ within the wall-normal distance in the range of $10^2 < y/\nu < 10^5$ and the streamwise velocity in the range of $0 < U < 1$. Data in $y^+ < 10$ are precluded because no wall model would be needed when the small scales are also resolved. Data above $y/\delta = 0.1$ are not included for training because the flow away from the wall is usually resolved by LES grids. Therefore, we have $10/u_\tau < y/\nu < 0.1Re_\tau/u_\tau$. For comparison purposes, we assume $u_\tau \approx 0.05$ and $0 < U < 1$, which are the same as the DNS data. Then we get the approximate range of y/ν . 501 points are selected evenly in the streamwise velocity range and 201 points are selected evenly in two adjacent orders of magnitude of y/ν , so that the training data contains about 501×603 input-output pairs. The neural network is trained to predict the friction velocity for given velocity and wall-normal distance. The inputs for training the neural network, which are defined based on the expression of the LOG-EXP formula as shown in Eq. 3, are shown in Table IV.

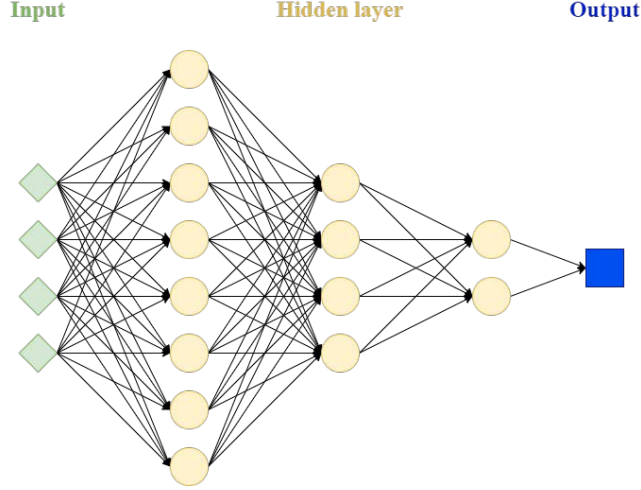


FIG. 11. Schematic diagram of the feedforward neural network (FNN) with multi hidden layers.

NN	AF	HL size	Input	Output
FNN	tanh	(8 ,4 ,2)	$\frac{1}{\kappa} \ln(1 + \frac{\kappa y U}{\nu}), A(1 - e^{-\frac{y U}{\nu B}}), C(1 - e^{-\frac{y U}{\nu D}}), \sqrt{\frac{y U}{\nu}}$	$\frac{U}{u_\tau}$

TABLE IV. Details of the neural networks. Here NN denotes neural network, AF activation function and HL hidden layer. The tabulated hidden layer size contains the number of neurons within each hidden layer.

Figure 12 (a) shows the friction velocity predicted by the FNN model, as a function of the streamwise velocity and the wall-normal distance divided by the kinematic viscosity. As seen in Figure 12 (b), the relative error of the friction velocity, which is define by

$$u_{\tau RE} = \frac{|u_\tau - u_{\tau FNN}|}{u_\tau}, \quad (18)$$

where u_τ and $u_{\tau FNN}$ are calculated by Eq. 3 and FNN, respectively, is smaller than 0.5% for most cases. And the relative error of the velocity in wall units obtained by FNN is smaller than 1%, except for the case when the streamwise velocity is very small. Then we test the FNN model using the DNS data of turbulent channel flow with $Re_\tau = 1000^{35}$. As seen in Figure 13, the predictions from the FNN model fit well with the DNS data for different wall-normal distannces.

REFERENCES

¹S. B. Pope, *Turbulent flows* (Cambridge University Press, Cambridge, 2001).

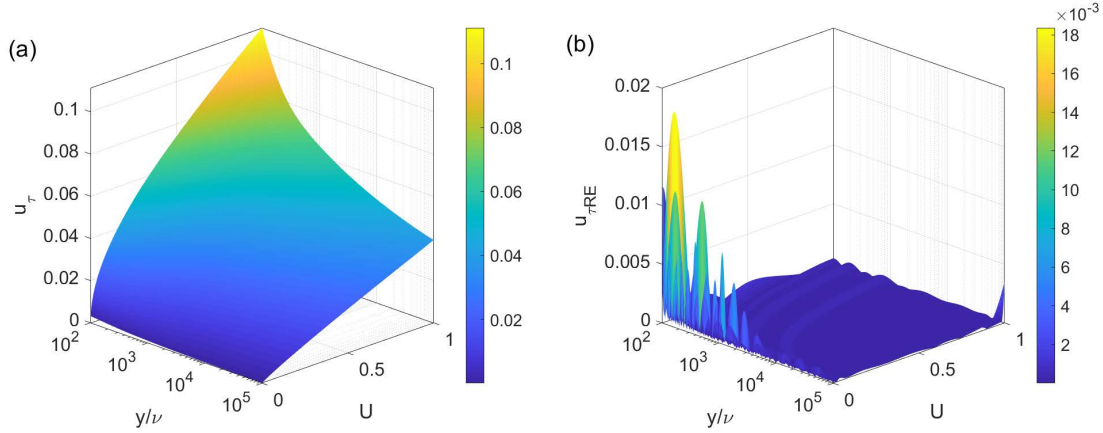


FIG. 12. Test of the FNN model using the data from the LOG-EXP formula for (a) the friction velocity and (b) relative error of the friction velocity predicted by FNN.

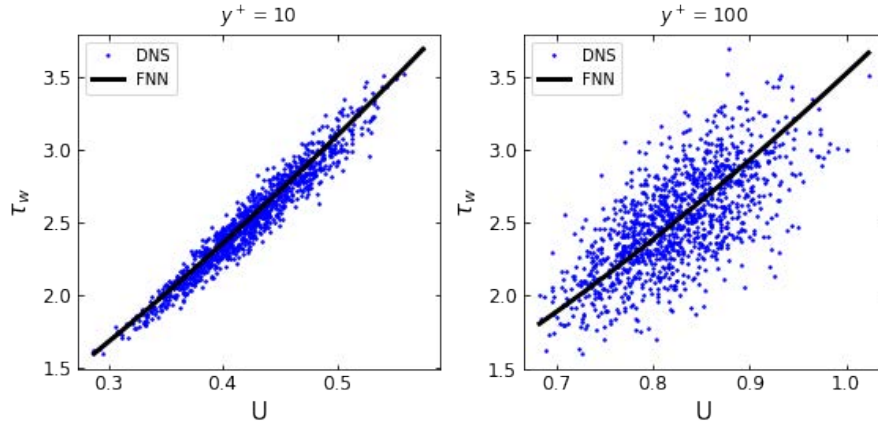


FIG. 13. Test of the FNN model using the DNS data of turbulence channel flow at $Re_\tau = 1000$ for (a) Wall shear stress as a function of the off-wall velocity at $y^+ \approx 10$ and (b) Wall shear stress as a function of the off-wall velocity at $y^+ \approx 100$.

²P. A. Davidson, *Turbulence: an introduction for scientists and engineers* (Oxford university press, 2015).

³L. Prandtl, “Eine beziehung zwischen warmeaustausch und stromungswiderstand der flussigkeiten,” *Phys. Z.* **11**, 1072–1078 (1910).

⁴G. I. Taylor, “Conditions at the surface of a hot body exposed to the wind,” *Rep. Memo. of the British Advisory Committee for Aeronautics* **272**, 423–429 (1916).

⁵v. Kármán, “The analogy between fluid friction and heat transfer,” *Transactions of the American Society of Mechanical Engineers* **61**, 705–710 (1939).

- ⁶R. G. Deissler, *Analysis of turbulent heat transfer, mass transfer, and friction in smooth tubes at high Prandtl and Schmidt numbers*, Vol. 1210 (National Advisory Committee for Aeronautics, 1954).
- ⁷W. D. Rannie, "Heat transfer in turbulent shear flow," *Journal of the Aeronautical Sciences* **23**, 485–489 (1956).
- ⁸M. Breuer and W. Rodi, "Large eddy simulation for complex turbulent flows of practical interest," in *Flow simulation with high-performance computers II* (Springer, 1996) pp. 258–274.
- ⁹H. Werner and H. Wengle, "Large-eddy simulation of turbulent flow over and around a cube in a plate channel," in *Turbulent shear flows 8* (Springer, 1993) pp. 155–168.
- ¹⁰M. Inagaki, O. Murata, T. Kondoh, and K. Abe, "Numerical prediction of fluid-resonant oscillation at low mach number," *AIAA journal* **40**, 1823–1829 (2002).
- ¹¹H. Reichardt, "Vollständige darstellung der turbulenten geschwindigkeitsverteilung in glatten leitungen," *ZAMM-Journal of Applied Mathematics and Mechanics/Zeitschrift für Angewandte Mathematik und Mechanik* **31**, 208–219 (1951).
- ¹²D. B. Spalding, "A single formula for the "law of the wall"," *Transaction of the Asme Journal of Applied Mechanics* **28**, 455 (1961).
- ¹³M. Rasmussen, "On compressible turbulent boundary layers in the presence of favorable pressure gradients," *American Society of Mechanical Engineers* (1975).
- ¹⁴A. Musker, "Explicit expression for the smooth wall velocity distribution in a turbulent boundary layer," *AIAA Journal* **17**, 655–657 (1979).
- ¹⁵R. Dean, "A single formula for the complete velocity profile in a turbulent boundary layer," *Journal of Fluids Engineering* (1976).
- ¹⁶P. A. Monkewitz, K. A. Chauhan, and H. M. Nagib, "Self-consistent high-reynolds-number asymptotics for zero-pressure-gradient turbulent boundary layers," *Physics of Fluids* **19**, 115101 (2007).
- ¹⁷E. R. Van Driest, "On turbulent flow near a wall," *Journal of the aeronautical sciences* **23**, 1007–1011 (1956).
- ¹⁸C. Duprat, G. Balarac, O. Métais, P. M. Congedo, and O. Brugière, "A wall-layer model for large-eddy simulations of turbulent flows with/out pressure gradient," *Physics of Fluids* **23**, 015101 (2011).
- ¹⁹B. J. Cantwell, "A universal velocity profile for smooth wall pipe flow," *Journal of Fluid Mechanics* **878**, 834–874 (2019).

- ²⁰J. C. Rotta, “Das in wandnhe gültige geschwindigkeitsgesetz turbulenter strömungen,” *Ingenieur-Archiv* **18**, 277–280 (1950).
- ²¹P. Anderson, W. M. Kays, and R. J. Moffat, “The turbulent boundary layer on a porous plate: an experimental study of the fluid mechanics for adverse free stream pressure gradients,” (1972).
- ²²L. Purtell, P. Klebanoff, and F. Buckley, “Turbulent boundary layer at low reynolds number,” *The Physics of Fluids* **24**, 802–811 (1981).
- ²³NICKELS and B. T., “Inner scaling for wall-bounded flows subject to large pressure gradients,” *Journal of Fluid Mechanics* **521**, 217–239 (2004).
- ²⁴J. H. Haritonidis, “A model for near-wall turbulence,” *Physics of Fluids A Fluid Dynamics* **1**, 302–306 (1989).
- ²⁵A. Yakhot, V. D. Khait, and S. A. Orszag, “Analytic expression for the universal logarithmic velocity law,” *Journal of Fluids Engineering* **115** (1993).
- ²⁶G. Nikuradse, “Laws of turbulent flow in smooth pipes,” (1966).
- ²⁷T. Cebeci and P. Bradshaw, *Physical and Computational Aspects of Convective Heat Transfer* (Springer-Verlag, 1984).
- ²⁸M. Lee and R. D. Moser, “Direct numerical simulation of turbulent channel flow up to $Re_\tau \approx 5200$,” arXiv preprint arXiv:1410.7809 (2014).
- ²⁹J. Laufer, “The structure of turbulence in fully developed pipe flow,” National Advisory Committee for Aeronautics Report (1953).
- ³⁰G. Charnay, G. Comte-Bellot, and J. Mathieu, “Development of a turbulent boundary layer on a flat plate in an external turbulent flow(effect of quasi-external isotropic turbulence on turbulent boundary layer development on flat plate),” *AGARD Turbulent Shear Flows 9 p(SEE N 72-20273 11-12)* (1972).
- ³¹E. R. Lindgren and J. Chao, “Average velocity distribution of turbulent pipe flow with emphasis on the viscous sublayer,” *The Physics of Fluids* **12**, 1364–1371 (1969).
- ³²X. Yang, F. Sotiropoulos, R. J. Conzemius, J. N. Wachtler, and M. B. Strong, “Large-eddy simulation of turbulent flow past wind turbines/farms: the virtual wind simulator (VWiS),” *Wind Energy* **18**, 2025–2045 (2015).
- ³³X. Yang and F. Sotiropoulos, “A new class of actuator surface models for wind turbines,” *Wind Energy* **21**, 285–302 (2018).
- ³⁴M. Germano, U. Piomelli, P. Moin, and W. H. Cabot, “A dynamic subgrid-scale eddy viscosity model,” *Physics of Fluids A: Fluid Dynamics* **3**, 1760–1765 (1991).

- 321 ³⁵J. Graham, K. Kanov, X. Yang, M. Lee, N. Malaya, C. Lalescu, R. Burns, G. Eyink, A. Szalay,
322 R. Moser, *et al.*, “A web services accessible database of turbulent channel flow and its use for
323 testing a new integral wall model for les,” *Journal of Turbulence* **17**, 181–215 (2016).
- 324 ³⁶I. Goodfellow, Y. Bengio, A. Courville, and Y. Bengio, *Deep learning*, Vol. 1 (MIT press Cam-
325 bridge, 2016).
- 326 ³⁷D. E. Rumelhart, G. E. Hinton, and R. J. Williams, “Learning representations by back-
327 propagating errors,” *nature* **323**, 533–536 (1986).
- 328 ³⁸D. P. Kingma and J. Ba, “Adam: A method for stochastic optimization,” *arXiv preprint*
329 *arXiv:1412.6980* (2014).
- 330 ³⁹F. Chollet, *Deep learning with Python*, Vol. 361 (Manning New York, 2018).